Radiation Monitoring in Mixed Environments at CERN: From the IRRAD6 Facility to the LHC Experiments

F. Ravotti, *Member, IEEE*, M. Glaser, A. B. Rosenfeld, *Senior Member, IEEE*, M. L. F. Lerch, A. G. Holmes-Siedle, *Senior Member, IEEE*, and G. Sarrabayrouse, *Member, IEEE*

***Abstract*—RadFET and *p-i-n* diode semiconductor dosimeters from different manufacturers will be used for radiation monitoring at the Experiments of the CERN LHC accelerator. In this work these sensors were exposed over three months in the CERN-IRRAD6 facility that provides mixed high-energy particles at low rates. The aim was to validate the operation of such sensors in a radiation field where the conditions are close to the ones expected inside full working LHC particle detectors. The results of this long-term irradiation campaign are presented, discussed and compared with measurements by other dosimetric means as well as Monte Carlo simulations. Finally, the integration of several dosimetric devices in one sensor carrier is also presented.**

***Index Terms*—Accelerators, dosimetry, MOSFET, particle beams, *p-i-n* diodes, proton, RadFET, radiation damage.**

I. Introduction

THE measurement of the radiation environment generated by proton-proton collisions at the High Energy Physics (HEP) Experiments of the CERN Large Hadron Collider (LHC) accelerator [1], has become an important issue over the last few years.

For the survey of the cumulative radiation damage in detectors and electronic devices [2] at the LHC, the mixed environment constituted of electromagnetic and hadronic radiation, will be constantly monitored with dosimetry of absorbed dose and fast particle fluence.

It has been already shown that semiconductor sensors can be successfully employed to characterize mixed radiation fields in terms of Ionizing Energy Loss (IEL) measured in SiO_2 and Non-Ionizing Energy Loss (NIEL) causing atom displacement within the silicon lattice. This can be achieved by combining two type of devices: RadFET transistors and *p-i-n* silicon diodes respectively [3].

Manuscript received September 27, 2006; revised January 11, 2007.

F. Ravotti is with the Technical Support Department, CERN, Geneva 23, CH-1211, Switzerland, and also with IES-University Montpellier II, F-34095 Montpellier Cedex 5, France (e-mail: federico.ravotti@cern.ch).

M. Glaser is with the Physics Department, CERN, Geneva 23, CH-1211, Switzerland.

A. B. Rosenfeld and M. F. L. Lerch are with the Center for Medical Radiation Physics, University of Wollongong, Wollongong 2522, NSW, Australia.

A. G. Holmes-Siedle is with REM Oxford, Ltd., Eynsham, Witney, OX29 4PD, U.K.

G. Sarrabayrouse is with the LAAS-CNRS, F-31077 Toulouse Cedex 4, France.

Color versions of one or more of the figures in this paper are available online at http://ieeexplore.ieee.org.

Digital Object Identifier 10.1109/TNS.2007.892677

The RadFET dosimeter operates by the build-up of "oxide-trapped charge," positive charge in the gate silicon oxide layer of the transistor [4]. This charge, responsible for the shift of the transistor threshold voltage, is stored internally, allowing the measurement of the deposited Total Ionizing Dose (TID) over several years. The *p-i-n* diodes are junction devices with a base of high-resistivity n-type silicon [5]. Hadron irradiation of such diodes produces displacement damage in the silicon base leading to an increase of the diode's forward voltage which is proportional to particle fluence [6].

In the HEP Experiments of the LHC, the use of these semiconductor technologies, as well as their integration on a sensor Printed Circuit Board (PCB), has already been proposed [7] and is now described. Semiconductor sensors suitable for the LHC must work over a very long time (10-years) and in challenging conditions including:

- particle runs of variable intensity with monthly shutdown periods;
- radiation compositions varying with the distance and the angle with respect to the interaction point;
- differing operating temperature in different measurement sites.

It is thus clear that the sensors for the LHC have to cover different sensitivities and a broad dynamic range in terms of TID and particle fluence as well as to comply with specific stability [8], [9] and response [10] requirements. For all these reasons, after intensive test campaigns, a series of four devices (two RadFETs and two *p-i-n* diodes) has been proved to fulfill LHC Experiments needs [11].

In this work the performances of the above four semiconductor sensors were validated by placing them in a low-rate, mixed-particle accelerator environment that simulated the working conditions at the LHC.

In the CERN facility IRRAD6 of the PS accelerator this was achieved by working off-axis in the 23 GeV proton beam-line directed to the IRRAD1 irradiation area [14]. Placing the sensors at different distances from the beam axis, various rates of high-energy photons, neutrons and charged particles in the GeV energy range were simultaneously available. Moreover, changes of beam conditions and the alternation of operation and shutdown periods, made this facility an ideal test-bench to validate stability over time.

Finally, this article will also present the integration of the employed sensors in a general-purpose chip carrier and PCB suitable for the LHC needs in terms of dimensions and material budget.

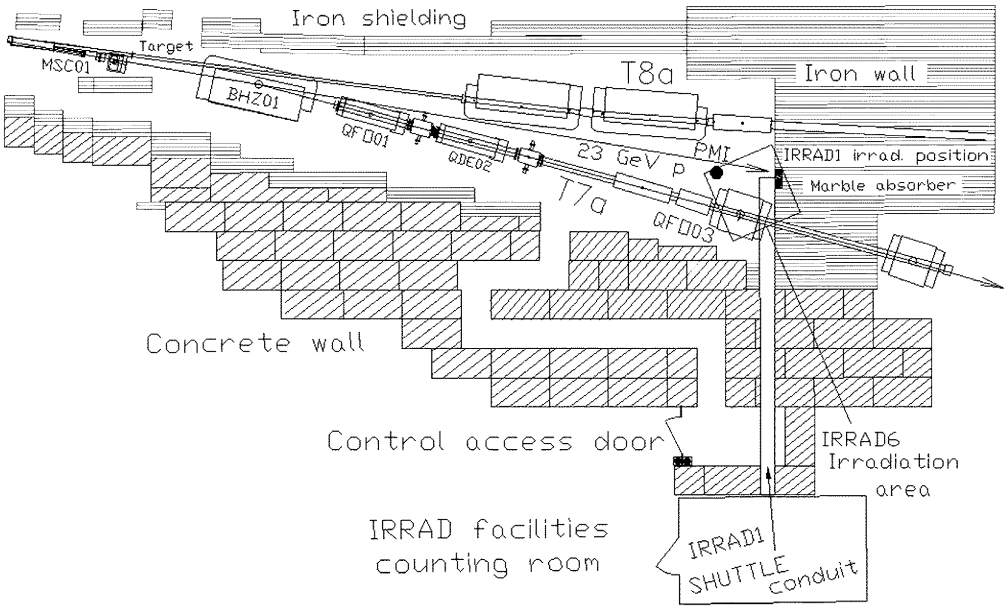

Fig. 1. Layout of the IRRAD facilities at the CERN-PS Accelerator.

II. Experimental Details

A. Irradiation Facility

In the T7 beam-line of the *East-Hall* Experimental Area of the CERN-PS Complex, the primary 23 GeV proton beam of the PS accelerator can be directed through the area where the irradiation facilities are located. In this area, primary-proton bursts of 2×10^{11} particles each are delivered toward a marble absorber placed in front of a cast iron beam-dump as shown in Fig. 1. In that location, protons produce a uniform irradiation spot over a surface of about 2×2 cm^2 [14]. Typically from 2 to 4 proton bursts per machine cycle of 16.8s are extracted from the PS accelerator and delivered toward T7. This irradiation layout will be referred as "*Primary Beam conditions*" in the following.

The above conditions are used to perform irradiation of samples moved inside the T7 beam by means of a remote controlled shuttle (IRRAD1 facility). However, during the operation of IRRAD1, the 23 GeV proton interactions produce in the surrounding area a radiation field manly composed by neutrons, photons, pions and protons. This setup is known as the IRRAD6 facility.

Moving downstream along the T7 beam-line, another test-beam facility can run in order to provide the users with a non-separated lower-energy secondary particle beam composed by $p^+, \pi^\pm$, and $e^\pm$ [15]. This secondary beam is produced by inserting a thick target toward the 23 GeV proton beam and modifying the magnetic field of the BHZ01 element (see Fig. 1). In these conditions, particles from the target with a selected momentum are bent over the T7a beam-pipe located in the right-hand side with respect the IRRAD1 position. While the secondary beam is thus delivered to users, the IRRAD1 facility, and consequently the IRRAD6 environment, is reached by a degraded primary proton beam. This irradiation set-up will be referred as "*Secondary Beam conditions*" in the following.

The instrumentation available in the T7 area consist of a Secondary Emission Chamber (SEC) labeled MSC01 in Fig. 1 that provides a measurement of the intensity for the primary protons delivered to IRRAD1 [16]. An Ionization Chamber (labeled PMI in Fig. 1) is also installed on the roof of the irradiation area for measuring the dose-rate due to induced activity during maintenance operations.

B. Devices Tested

The RadFET dosimeters used in this work are those recommended for the LHC Experiments in the *Sensor Catalogue* document [11]. The supplier were the laboratory CNRS-LAAS, France [17] and REM in England [18]. These devices were all encapsulated in sealed TO-5 metal packages. The LAAS devices have been chosen for their sensitivity in the mGy dose range, while the REM devices have been selected because of their broad dynamic range. The recorded signal from RadFETs is the shift of the transistor threshold voltage $V_{\rm th}$ that is converted to dose D (Gy) following a power-low calibration curve $\Delta V_{\rm th} = a \cdot D^b$, where a and b are experimental parameters.

As showed in many works [8], [9] and in references therein, annealing phenomena [2] that affect the RadFETs selected in [11] are of the order of a few percent over years time-scale. For this reason the data presented in this work were not corrected for such a effect.

To measure the 1-MeV neutron equivalent particle fluence $\Phi_{\rm eq}$ (cm^{-2}), *p-i-n* diodes were supplied by CMRP, Australia [19]. Because of the very high sensitivity, these devices work in a limited fluence range up to about 2×10^{12} cm^{-2}. After that exposure level the signal loses its linearity with $\Phi_{\rm eq}$.

To extend the measurement range of $\Phi_{\rm eq}$ at higher values as required for the LHC, commercial BPW34 diodes from OSRAM, Germany [20] were also investigated and adopted as $\Phi_{\rm eq}$ sensors. Complementary to CMRP devices, the BPW34 show sensitivity to fast particles once $\Phi_{\rm eq}$ exceeds 2×10^{12} cm^{-2} [7].

TABLE I
SEMICONDUCTOR SENSORS CHARACTERISTICS IN THE MEASUREMENT RANGE OF INTEREST FOR THIS WORK

		REM	LAAS	CMRP	BPW34
		RadFET		*p-i-n*	
oxide/base thick.	μm	0.25	1.6	1000	$\sim$100
W/L ratio	μm	440/10	9500/37	-	-
Readout i	mA	0.16	0.10	1.0	1.0
Readout Δt	s	5.0	1.0	0.7	0.7
Initial $V_{th/F}$	V	2.9	2.6	3.1	0.5
Initial T_c	mV/°C	-0.6	-0.05	-21.4	-2.6
Max. Dose	Gy	530	10	-	-
Max. Φ_{eq}	cm^{-2}	-	-	$2x10^{12}$	$3x10^{13}$
Max. $V_{th/F}$	V	12.1	5.5	12.3	5.3
post-irrad. T_c	mV/°C	-2.3	$\sim$ -0.05	-0.8	-6.0
Calibration Data					
		$D < 20$ Gy			
a	V/Gy	0.018	0.515	-	-
b		0.911	0.481	-	-
		$D > 20$ Gy			
a	V/Gy	0.029	-	-	-
b		0.708	-	-	-
c^{-1}	cm^{-2}/mV	-	-	$1.7x10^8$	$9.1x10^9$
Calib. Error	$\pm$%	10	10	13	20

TABLE II
LOCATION OF TESTED DEVICES IN IRRAD6

Label	r = 60	r = 90	r = 100	PMI Loc.	Mag. QF003
Z (cm)	15	15	15	130	60
r (cm)	60	90	100	80	140

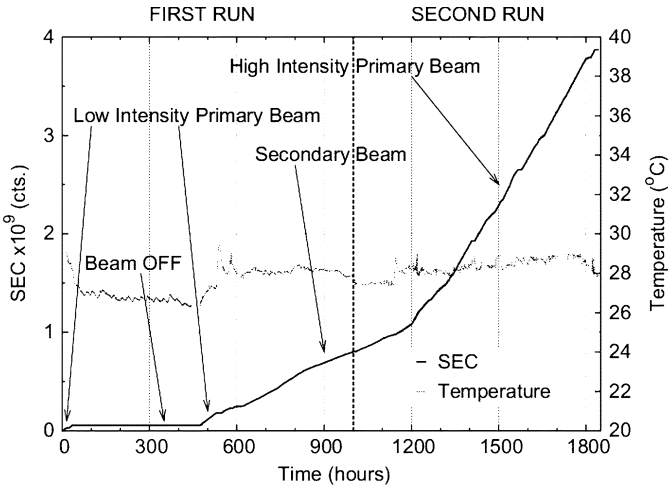

Fig. 2. Intensity of the 23 GeV proton beam delivered to T7.

For both *p-i-n* diodes the recorded dosimetric parameter is the shift of the forward voltage V_F that increases proportionally with the fluence following the equation:

$$\Delta V_F = c \cdot k \cdot \Phi = c \cdot \Phi_{\mathrm{eq}} \tag{1}$$

where *k* is the *hardness factor* allowing to compare the damage efficiency in silicon of different radiation sources [21], Φ is the total particle fluence and *c* is an experimental parameter.

Both RadFETs and *p-i-n* diodes were exposed in "zero bias" mode and the dosimetric parameters (voltages) were read-out by forcing different pulsed currents through them. The main characteristics of the sensors, together with their readout and calibration parameters a, b and c are listed in Table I. The data used as REM and BPW34 calibration curves come from different irradiation sources [11]. For CMRP and LAAS devices the existing data [11] were complemented with [12] and with recent data sets from the authors measured at the TRIGA nuclear reactor of the *Jozef Stefan Institute* in Ljubljana, Slovenia [13].

Before converting the voltages to dosimetric quantities, the recorded signals from the sensors were corrected against temperature variations using the set of T_c reported in Table I.

C. Irradiation Setup

RadFET and *p-i-n* diode sensors were placed at five measurement points in the IRRAD6 area facing the cast iron beam-dump as indicated in Fig. 1. Table II details the measurement positions as well as their labeling used in the discussion of the results. The coordinate *Z* is the distance from the beam-dump calculated along the beam-line, while *r* is the radial distance from the beam-axis.

Three measurement positions were chosen, at different radii ($r = 60, r = 90$ and $r = 100$), close to the marble absorber while the other two were in proximity of the beam-line element named QF003 (*Mag. QF003*) and the PMI Ionization Chamber (*PMI Loc.*) represented as black dot in Fig. 1.

Each sensor was then connected to the readout system via 25-m coaxial cable. LAAS RadFETs and both CMRP and BPW34 *p-i-n* diodes were installed in their array positions from the beginning of the irradiation test. REM RadFETs were instead added to the setup during an accelerator shut-down period 1000 hours after the beginning of the experiments.

All measurements employed an automated DAQ system consisted of a *Keithley Source Meter 2410* and an *Agilent Switch Matrix* WHICH commutes the sensors terminals between exposure and readout mode. The Source Meter was used as current generator and also to record the sensor voltages. Both units were under PC control by means of a LabVIEW program that periodically runs the sensors readout cycle.

III. RESULTS AND DISCUSSION

The irradiation period lasted about three months (1900 hours). The intensity of the primary 23 GeV proton beam delivered to the irradiation area in this period (in term of counts from the SEC) is shown in Fig. 2. During the test, the beam conditions in the T7 area were switched several times from *Primary* to *Secondary* beam and back, according to a pre-defined schedule. Therefore, to simplify the discussion of the results data have been grouped in two separate runs:

- *First Irradiation Run from 0 to 1000 hours*: After about 50 hours in which the PS beam was normally extracted and directed to the irradiation area (*Low Intensity Primary Beam*), a severe beam-line failure occurred and the T7 beam-line was shut down for about 500 hours (*Beam OFF*). Then, after about 100 hours from the recovery of the beam

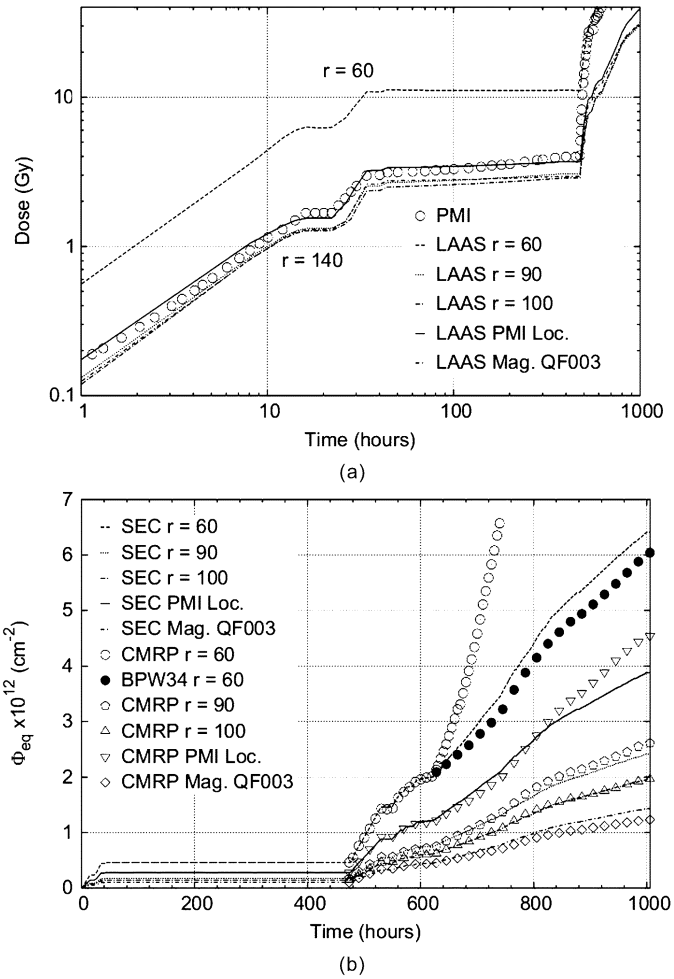

Fig. 3. Radiation measurements during the first irradiation run. (a) Radiation dose. (b) Equivalent fluence.

(i.e., 600 hours in Fig. 2) the T7 beam-line was setup for the delivery of the *Secondary Beam*.

- *Second Irradiation Run from 1000 to 1900 hours*: The setup for the *Secondary Beam* was maintained for the first 200 hours before changing back to the *Primary Beam* conditions until the end of the experimental run. In this last part, starting from 1200 hours, the proton intensity was about twice the previous one (*High Intensity Primary Beam*).

The average temperature recorded in the test area was of 28° C $\pm 1.5°$ C as shown in the secondary y-axis of Fig. 2.

A. First Irradiation Run

1) Measurements: Fig. 3 shows all measurements recorded during the first irradiation run. In Fig. 3(a) the doses measured with the LAAS devices have been plotted with different lines for the various locations. The dose recorded with a LAAS device at the PMI Location is compared with the one directly measured with the PMI Ionization Chamber (circular markers in Fig. 3(a)). The agreement of the two measurements is very good for absorbed doses <10 Gy.

It has to be noted that, even if the operation with protons was suspended during the period from 50 to 500 hours, the sensors were exposed at the PMI location to a residual dose-rate of about 2 mGy/h due to scattered particles from the neighboring secondary beam-lines running in the *PS East-Hall*. During this period the signal of the LAAS devices continued to increase even at this very low dose-rate, demonstrating the high sensitivity of such devices. Once the operation with protons restarted, the dose-rate in the area increases to a level that saturates the PMI readout electronics (>400 mGy/h), making a further use of this signal as a reference for the devices under test impossible [22].

In Fig. 3(b) the $\Phi_{\rm eq}$ recorded by the CMRP devices have been plotted with open markers. To verify the linearity in the response of these devices, the experimental data were linearly fitted by scaling the proton beam intensity of Fig. 2 with a series of conversion factors m_i (SEC counts $\mapsto \Phi_{\rm eq}$) for any given measurement locations. The results of these calculations are plotted with different lines in Fig. 3(b). For all CMRP devices, the measurements fit well the data over the entire run when $\Phi_{\rm eq}$ is lower than the sensor's dynamic range (i.e., $<2 \times 10^{12}$ cm^{-2}). Even for the location in which the particle flux was the less intense (*Mag. QF003* plotted with diamond markers) the sensor behaves linearly with the calculation, proving that annealing phenomena that could affect such devices are lower than the measurement error.

For the measurement position $r = 60$ on Fig. 3(b), in which the flux of particle was the highest recorded, the signal of the BPW34 diode has been plotted with filled circular markers. This signal has been normalized to the last measurement point of the CMRP device at $\Phi_{\rm eq} = 2 \times 10^{12}$ cm^{-2}. The BPW34 signal is in agreement with the calculation (dotted line) within the calibration error (20%) if, already for this relative high particle intensity, the raw data are corrected against both short- and long-term annealing phenomena. For the present work, the annealing corrections have been based on annealing data recorded after irradiation [23] and from some independent results [12]. A more detailed characterization of the annealing of the BPW34 devices in presently underway at CERN.

2) Comparison With Monte Carlo Simulations: To validate the absolute $\Phi_{\rm eq}$ presented in Fig. 3(b), the CMRP results have been compared with two sets of Monte Carlo simulations performed for IRRAD6 [24]. The two simulations, labeled *Sim 50k* and *Sim 100k*, differ in the number of generated primary events (5×10^4 and 1×10^5 primary 23 GeV protons respectively) and slightly in the layout and materials used to model the T7 area. Moreover, while the *Sim 50k* has been run for different pairs of coordinates r and Z, the *Sim 100k* predicts only the variation of the radiation field along the radius from the beam axis at a fixed Z of 15 cm.

To compare particle fluence measurements and simulations, the set of scale parameters m_i previously calculated in Section III-A.1 (1-MeV$_{\rm eq}$ part./(cm$^2\times$ counts)) were normalized to the intensity of a single primary proton burst (1-MeV$_{\rm eq}$ part./(cm$^2\times$ spill)). Knowing the *hardness factor* for the IRRAD6 area it is then possible, via (1), to express the experimental data in terms of part./(cm$^2\times$ spill) and proceed with the comparison.

Fig. 4(a) show the particle spectra predicted with the *Sim 100k* for the measurement position $r = 60$. In this location the neutron component appears already to dominate with respect to the

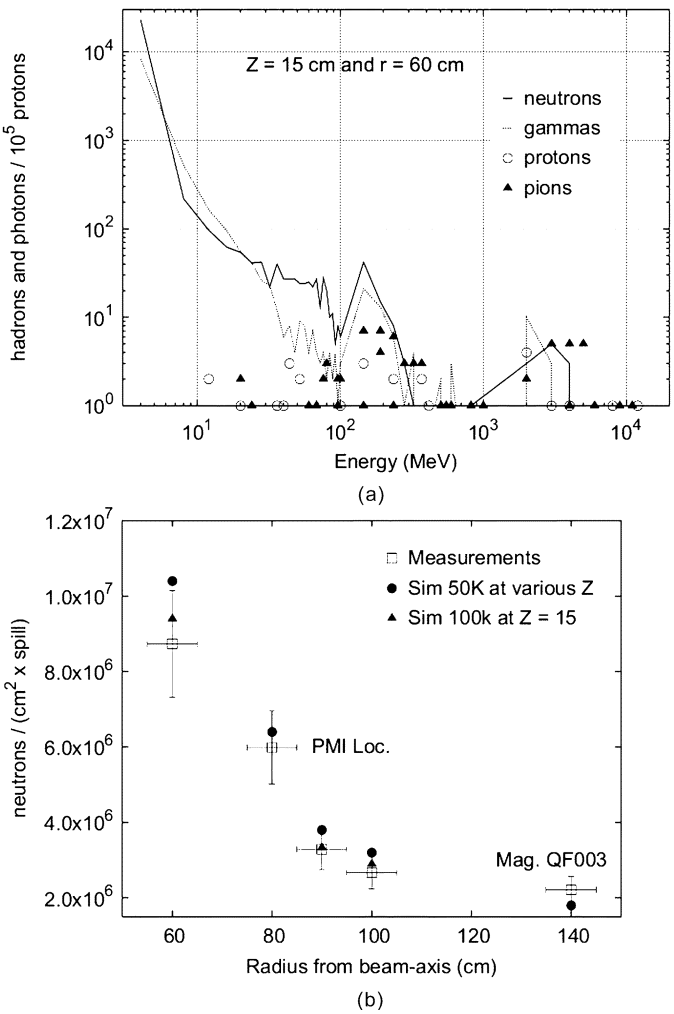

Fig. 4. Monte Carlo simulations for IRRAD6 operated with *Primary Beam*. (a) Particle Spectra from *Sim 100 k* at Z $= 15$ cm and r $= 60$ cm, (b) Comparison between simulations and the CMRP measurements.

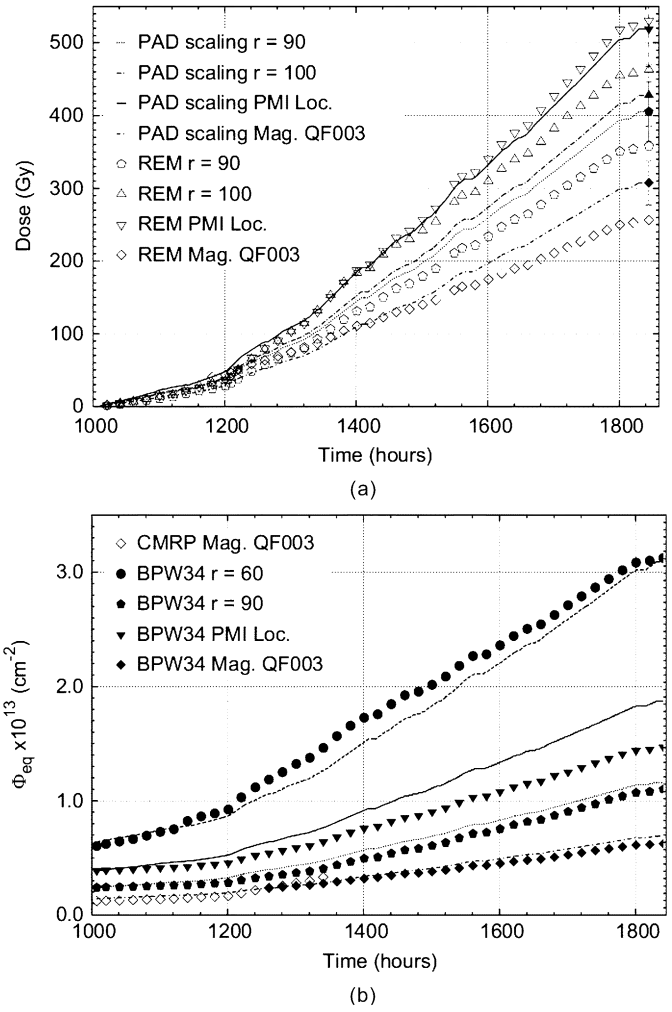

Fig. 5. Radiation measurements during the second irradiation run. (a) Radiation dose. (b) Equivalent fluence.

charge particles that represent only a few percent of the total number of particles. The *hardness factor* was calculated to be $k = 1.21 \pm 0.11$ folding the neutron spectra of Fig. 4(a) with known neutron NIEL Kerma factors [21]. The error calculated for k takes into account the contribution of the charged particles to NIEL and the energy variation in the simulated neutron spectra moving in IRRAD6 from 60 cm to 140 cm in radius from the beam axis.

Fig. 4(b) shows the comparison between the measurements carried out using the diodes (open markers) with the two simulations (filled markers). The error associated to the measurement $(\pm 16.2\%)$ takes into account the uncertainties in the CMRP diodes calibration (see Table I) as well as the one in the evaluation of the k factor. The data of the *Sim 100k* (triangle markers in Fig. 4(b)) are only available for Z $= 15$ while the *Sim 50k* has been run for different Z values (round markers). At positions closest to the beam axis, the Monte Carlo simulations overestimate the experimental measurements. This finding is in agreement with [25] where similar results where found by means of experimental measurements using activation foils [26]. The *Sim 50k* are shown to be overestimated with respect to the experimental measurement up to more than 20% for the closest position to beam-axis where the higher particle gradient may enhance the errors of both measurements and simulations. The *Sim 100k* shows instead an agreement better than 10% with the experiments. These two results confirm thus the validity of CMRP diode measurements.

B. Second Irradiation Run

Fig. 5 shows all measurements recorded during the second irradiation run. In Fig. 5(a) the results from REM devices have been compared with the TID measurements carried out with Polymer-Alanine dosimeters (PAD) [27]. In the figure, the PAD measurements are the filled markers at 1900 hours, while the lines are the scaling of the dose from PADs using the proton intensity plotted in Fig. 2. The TID values measured from RadFETs agree for all positions with PAD measurements within an experimental error of $\pm 10\%$. The choice of PAD dosimeters to validate the measurement from REM RadFETs become clear if the contribution to the TID of photons (γ), neutrons (n) and charged hadrons (*Ch.H*) in the mixed radiation field are considered separately as shown in (2) and (3). In the formulas, K_i^j are

the IEL Kerma factors [28]–[30] where $i = \gamma, n$ or *Ch.H* and $j = \mathrm{P}$ for PAD or R for REM devices. Φ are instead the different particle fluences, while the numerical factors take into account the relative neutrons sensitivity of the two dosimeters with respect to the gamma rays.

$$\mathrm{D_{PAD}} = \mathrm{K}_{\gamma}^{P} \times \Phi_{\gamma} + (0.2) \times \mathrm{K}_{n}^{P} \times \Phi_{n} + \mathrm{K}_{Ch.H}^{P} \times \Phi_{Ch.H} \tag{2}$$

$$\mathrm{D_{REM}} = \mathrm{K}_{\gamma}^{R} \times \Phi_{\gamma} + (0.6) \times \mathrm{K}_{n}^{R} \times \Phi_{n} + \mathrm{K}_{Ch.H}^{R} \times \Phi_{Ch.H}. \tag{3}$$

From the tabulated K_i^j factors it is easy to verify that, in the energy range from 4 MeV to several GeV, even if from Fig. 4(a) it is that $\Phi_{Ch.H} \sim 0.1 \times \Phi_n \sim 0.1 \times \Phi_\gamma$, the charged particle component delivers to both PAD and REM about the same TID two order of magnitude higher than the one deposed by neutrons and photons. In such conditions PAD dosimeters are expected to be a good benchmark for the REM dosimeters.

With different filled markers, Fig. 5(b) shows the Φ_{eq} measurements recorded by the BPW34 diodes. The scaling of the primary beam intensity for any measurement location, as calculated in Section III-A.1, has been again plotted with lines for comparison with the experimental data. As previously pointed out, with the opportune annealing correction, the signal of such a devices match, in all cases, the predicted Φ_{eq} within the uncertainty of about $\pm 20\%$ that affects the calibration data.

C. Discussion of the Ratio "REM Response/LAAS Response" or "R/L Ratio"

In the second irradiation run, the responses from the LAAS devices, already exposed to a TID exceeding some tens of Gy during the first run, are of interest. For doses exceeding 10 Gy their response curve becomes strongly sub-linear, i.e., begins to saturate. Although the responses of all MOSFETs under "zero bias" are always strongly sub-linear [10], the REM devices at the same total dose are not saturating in this way. The saturation mechanism is not well understood but it is clear that further electron escape might be retarded by built-in oxide fields due to oxide-trapped positive charge [31]. At a TID of 500 Gy, saturation of LAAS devices is nearly complete. The REM devices have been instead proven to have smoothly rising radiation response curves over a range of several tens of kGy under exposure to many different types of radiation [11].

In Fig. 6, we show the "R/L ratio," i.e., the sensitivity of the REM devices with respect the LAAS ones during the second irradiation run. *Primary Beam* registers a ratio of 3, while the *Secondary Beam* registers a factor of 2. In GeV proton experiments, it may be of practical benefit to monitor the "R/L ratio," as will be explained later.

As with the saturation effects in zero-bias cases, the exact mechanism of the clear-cut change in "R/L ratio" is not clear. The explanation is likely to arise from the plentiful creation of secondary (scattered) protons and other charged particles in the second case. This is because the *Secondary Beam* has been scattered from a thick target placed in the primary beam.

The number of secondaries in the IRRAD6 area is known to scale with the number of particles directed to the beam-dump,

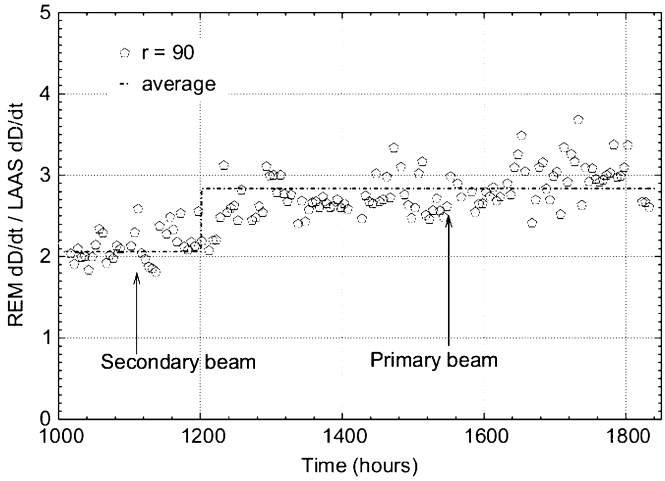

Fig. 6. Sensitivity "R/L ratio" for RadFETs REM and LAAS during the second irradiation run. Plot relative to the couple of sensors installed at $\mathrm{r} = 90$.

and these are duly counted by the SEC. However, many aspects of beam focusing are altered so that the beam-spot geometry changes. Many new possibilities of generating neutrons and photons at the measurement locations in IRRAD6 are created. In addition, the proton energies have degraded to just the region where previous workers [31], [32] have discovered severe dependence of the MOSFET response on particle LET.

Further work is needed to decide whether the ratio changes more due to average proton LET (we could call this "softening" of the proton beam) or to the addition of photons and neutrons to the beam which, given their high LETs [2], we could describe as "dilution" of the beam.

This finding suggests, using these RadFETs at the LHC, to monitor the REM/LAAS signal ratio to uncover important variations in the composition of the beam. Furthermore, during full LHC particle experiments, monitoring it may be able to give useful warnings of partial beam loss or bad beam tuning conditions.

IV. Sensor Carrier for the LHC Experiments

Section III can be said to validate the proposal to employ a set of the four sensors to guarantee the complete monitoring of a mixed environment as expected inside the LHC Experiment areas [7].

To allow easy handling and to provide a standard connectivity for all proposed sensors, an integrated PCB carrier was designed and produced at CERN as shown in Fig. 7. This carrier is made of a thin (200 μm) double-sided PCB. It can host up to 5 *p-i-n* diodes in the places labeled from D1 to D5 in Fig. 7. In the middle of Fig. 7(a), the sensor mounted at the top is a CMRP diode, while the bottom one is a BPW34 diode sealed in a DIL package.

The PCB carrier can also allow the readout of five other devices hosted inside a proper package. At the moment, a series of packages containing four RadFETs have been designed and produced for the LHC Experiments. One of these can be seen, mounted on the sensor PCB, on the right-hand side of Fig. 7(a). A temperature probe (see S1 in Fig. 7(b)) is also provided. The

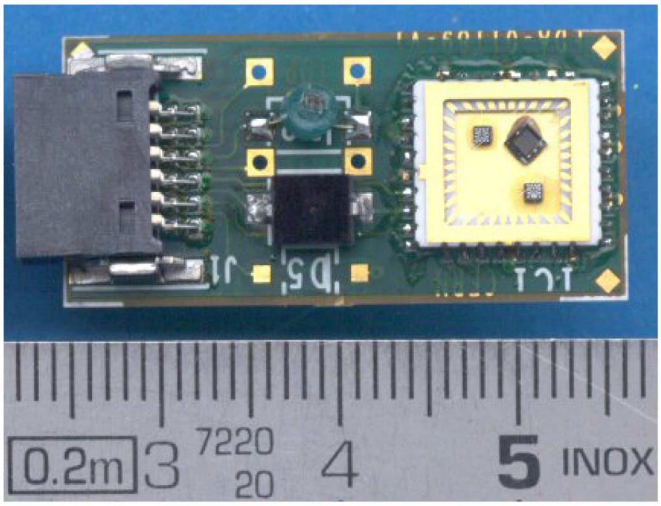

(a)

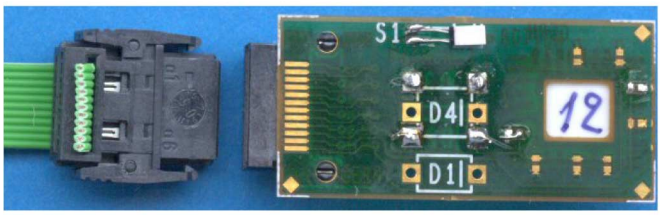

(b)

Fig. 7. Integrated sensor carrier for the LHC Experiments. (a) PCB Front-side with 2 *p-i-n* diodes and 3 RadFET dies on board, (b) PCB Back-side with external cabling.

11 devices mounted on the integrated sensor PCB can be read out via a 12-way flat cable (11 for sensor signals and a common GND connection) as shown in the left-hand side of Fig. 7(b). The overall dimensions of the assembled PCB, including the connector plug, are of about $34 \times 15 \times 4$ mm^3.

It has been shown [10], [32] that the distribution and composition of the materials around RadFETs can strongly interfere with TID measurements, especially in radiation fields containing neutrons and/or low energy photons. Dose enhancement effects are thus an issue. Moreover, the space available for the installation of such kind of sensors is another important constraint in the case of the LHC. For this reason, many of the chip packages used for RadFETs in other applications may well be unsuitable for a direct application at the LHC, therefore the special ceramic carrier for the REM and LAAS sensors was designed to face these issues [33].

It is a 36-pin, ceramic SM carrier of less than 10 mm^2 surface and of about 1.3 mm thickness. A thin membrane, usually made of aluminum or polyimide, is used as carrier lid (not shown in Fig. 7(a)). This supplies protection from dust and mechanical damage keeping low its mass. The carrier hosts 4 die for a total of 10 different RadFETs dosimeters. However, mounting it on the PCB carrier, wiring can be supplied to four MOSFET elements at one time. During assembly, a selection of the elements to be read out is made via the sets of connection pads visible in the right-hand side of Fig. 7(b). By soldering together or floating two adjacent pads it is possible to enable or disable respectively the readout of a specific element.

The sensor signals are read via the flat cable and the connector plug. However, a less cumbersome method is to directly solder the flat cable to the PCB using the pads located under the connector plug shown in Fig. 7(b).

V. Conclusion

The rate and the particle mix described for the irradiation test at the CERN IRRAD6 facility, gave integrated doses of several hundred Gy and particle fluences exceeding 10^{13} cm^{-2} over 1900 hours. These irradiation levels, together with some variations of the particle beam in time and in its tuning, were very effective as simulation of the LHC working conditions. The four semiconductor sensors tested in IRRAD6 are recommended for internal radiation monitoring throughout the 10 years of LHC experiments. These sensors would be placed within the detectors grouped around the interaction points. The set of four devices are: RadFETs manufactured by REM and CNRS-LAAS and *p-i-n* diodes from CMRP and OSRAM. These worked successfully in the simulated mixed-particle environment.

The accuracy achieved in the measurement of dose (TID) and 1-MeV neutron equivalent fluence, falls within the experimental calibration errors (10% to 15%) for REM, LAAS and CMRP devices. Previous calibrations of these devices were tests in relatively "high-rate" irradiation where annealing phenomena have been not explicitly considered. In the case of the BPW34 diodes the measurements have been found to be in agreement within 20% only if opportune annealing corrections are used. With further annealing studies, the accuracy of such a devices could be probably brought down at the level of the other sensors.

A new concept of using two RadFET sensors with very different oxide thicknesses has been discovered. Their signals at TID$>$10 Gy can be fruitfully used as complementary information to detect changes in the radiation field composition. This feature is thought to be a valuable indication of (intentional or accidental) changes in the LHC beam conditions induced by differing or faulty tuning of the primary beams.

The set of the four recommended sensors covers well the needs of the LHC Experiments in terms of sensitivity (3.5 mGy/mV,1.7 $\times$ 10^8 cm^{-2}/mV) and dynamic range ($>$20 kGy, 4×10^{14} cm^{-2}). The above studies justified the production of an integrated sensor PCB which is expected to simplify the handling of the radiation sensor set.

The signals from the integrated carrier can be remotely readout up to very long distances using cabled connections. However, as all mounted sensors keep stored the dosimetric information over time, the integrated PCB can be also used in a "passive" mode by exposing it to radiations with all connections grounded. For this latter application, the integrated sensor must be removed from the measurement field and plugged on a laboratory test-bench to perform the readout cycle.

While the present carrier was optimized for the LHC, the above features makes its utilization easily extendible to any application in which monitoring of cumulative dose and particle fluence is needed.

Acknowledgment

The authors would like to thank M. Moll from CERN for the review of the manuscript and his valuable contribution to im-

prove it and I. Mandic from the *Jozef Stefan Institute* of Ljubljana, Slovenia for his help in the calibration campaigns of the studied dosimeters. The TS-DEM group and the technicians of the PH-DT2 Bonding Lab at CERN are also gratefully acknowledged for their support in the design of the integrated sensor carrier and in the assembly of the SMD RadFET packaging respectively.

REFERENCES

[1] *The Large Hadron Collider Project Webpage [Online]*, [Online]. Available: http://www.cern.ch/lhc-new-homepage/, Available

[2] A. G. Holmes-Siedle and L. Adams*, Handbook of Radiation Effects (Second Edition)*. Oxford, U.K.: Oxford Univ. Press, 2002.

[3] A. B. Rosenfeld, M. I. Reinhard, D. Marinaro, P. Ihnat, G. Taylor, L. Peak, N. Freeman, D. Alexiev, and M. Lerch, "A system for radiation damage monitoring," *IEEE Trans. Nucl. Sci.*, vol. 46, no. 6, pp. 1766–1772, Dec. 1999.

[4] A. G. Holmes-Siedle and L. Adams, "RadFETs: A review of the use of metal-oxide-silicon device as integrating dosimeters," *Rad. Phys. Chem.*, vol. 28, no. 2, pp. 235–244, 1986.

[5] A. B. Rosenfeld, "PIN diodes with a wide measurement range of fast neutron dose," *Rad. Prot. Dos.*, vol. 33, no. 1–4, pp. 175–178, 1990.

[6] Z. Li, W. Chen, and W. Kraner, "Effects of fast neutron irradiation in the electrical proprieties of silicon detectors," *Nucl. Inst. Meth.*, vol. A308, pp. 585–595, 1991.

[7] F. Ravotti, M. Glaser, M. Moll, K. Idri, J.-R. Vaillé, H. Prevost, and L. Dusseau, "Conception of an Integrated Sensor for the Radiation Monitoring of the CMS Experiment at the Large Hadron Collider," *IEEE Trans. Nucl. Sci.*, vol. 51, no. 6, pp. 3642–3648, Dec. 2004.

[8] F. Ravotti and M. Glaser, "A study of the response of solid-state dosimeters to be used for the measurement of the radiation environment of the CMS experiment at the LHC," CERN Tech. Note EST-LEA-2003-03, 2003.

[9] F. Ravotti, M. Glaser, F. Saigné, L. Dusseau, and G. Sarrabayrouse, "Prediction of the thermal annealing of thick oxide metal-oxide-semiconductor dosimeters irradiated in a harsh radiation environment," *Appl. Phys. Lett.*, vol. 89, no. 8, Aug. 2006, 083503.

[10] F. Ravotti, M. Glaser, M. Moll, Ch. Ilgner, B. Camanzi, and A. G. Holmes-Siedle, "Response of RadFET dosimeters to high fluences of fast neutrons," *IEEE Trans. Nucl. Sci.*, vol. 52, no. 4, pp. 959–965, Aug. 2005.

[11] F. Ravotti, M. Glaser, and M. Moll, "Sensor Catalogue—Data compilation of solid-state sensors for radiation monitoring," CERN TS-Note-2005-002, May 13, 2005.

[12] G. Kramberger, V. Cindro, I. Mandic, M. Mikuz, and M. Zavrtanik, "Development of ATLAS Radiation Monitor." [Online]. Available: http://www.cern.ch/lhc-expt-radmon

[13] M. Ravnik and R. Jeraj, "Research reactor benchmarks," *Nucl. Sci. Eng.*, vol. 145, pp. 145–152, 2003.

[14] M. Glaser, F. Ravotti, and M. Moll, "Dosimetry assessments in the irradiation facilities at the CERN-PS accelerator," *IEEE Trans. Nucl. Sci.*, vol. 53, no. 4, pp. 2016–2022, Aug. 2006.

[15] D. J. Simon and L. Durieu, "Secondary beams for tests in the PS East experimental area," CERN PS/PA Note 93-21, Aug. 4, 1993.

[16] K. Bernier, G. de Rijk, G. Ferioli, E. Hatziangeli, A. Marchionni, V. Palladino, G. R. Stevenson, T. Tabarelli, and E. Tsesmelis, "Calibration of secondary emission monitors of absolute proton beam intensity in the CERN SPS north area," CERN Yellow Rep. 97-07, 1997.

[17] G. Sarrabayrouse and V. Polischuk, "MOS ionizing radiation dosimeters: From low to high dose measurements," *Rad. Phys. Chem.*, vol. 61, pp. 511–513, 2001.

[18] *Radiation Experiments and Monitors (REM) Webpage*, [Online]. Available: http://www.radfet.com

[19] *Univ. Wollongong, Center for Medical Radiation Physics (CMRP)*, [Online]. Available: http://www.uow.edu.au/eng/phys/rpg/

[20] *BPW34F photodiode datasheet. OSRAM Opto-Semiconductors*, [Online]. Available: http://www.osram-os.com

[21] "Standard practice for characterizing neutron energy fluence spectra in terms of an equivalent mono-energetic neutron fluence for radiation hardness testing of electronics," Nov. 1994, ASTM E722-94, ASTM Committee.

[22] H. Vincke. CERN SC-RP, Geneva, Switzerland, Feb. 2006, private communication.

[23] F. Ravotti, CERN TS-LEA, Geneva, Switzerland, 2004, unpublished.

[24] C. Leroy and P. Roy, "Calculation of particle fluxes in the PS silicon proton irradiation zone," 1998, UdeM-GPP-EXP-98-03.

[25] I. Bacardit-Corrons, "Flux measurement of hadrons using activation methods at CERN AD target area and at T7 irradiation facility," Diploma thesis, Univ. Politecnica Catalunya, Barcelona, Spain, 2000.

[26] S. Charalambus, J. Dutrannois, and K. Goebel, "Particle flux measurement with activation detectors," CERN DI/HP 90 Health Physics, Jul. 14, 1966.

[27] F. Coninckx, H. Schonbacher, M. Tavlet, G. Paic, and D. Razem, "Comparison of high-dose dosimetry systems for radiation damage studies in collider detectors and accelerators," *Nucl. Inst. Meth.*, vol. B83, pp. 181–188, 1993.

[28] M. B. Chadwick, "A consistent set of neutron kerma coefficients from thermal to 150 MeV for biologically important materials," *Med. Phys.*, vol. 26, pp. 974–991, 1999.

[29] J. H. Hubbell, "Photon mass attenuation and energy absorption coefficients from 1 keV to 20 MeV," *Int. J. Appl. Radiat. Isot.*, vol. 33, pp. 1269–1290, 1982.

[30] Particle Data Group, "Review of particle physics," *Eur. Phys. J. C*, vol. 15, pp. 1–878, 2000.

[31] R. Pease, M. Simons, and P. Marshall, "Comparison of pMOS total dose response for Co-60 gammas and high-energy protons," *IEEE Trans. Nucl. Sci.*, vol. 48, no. 3, pp. 908–912, Jun. 2001.

[32] S. Kronenberg and G. J. Brucker, "The use of hydrogenous material for sensitising pMOS dosimeters to neutrons," *IEEE Trans. Nucl. Sci.*, vol. 42, no. 1, pp. 20–26, Feb. 1995.

[33] R. Capra, S. Guatelli, M. Moll, M. Glaser, M. G. Pia, and F. Ravotti, "Simulation for LHC radiation background: Optimization of monitoring detectors and experimental validation," in *Proc. Comput. High Energy Nucl. Phys. (CHEP 2006)*, Mumbai, India, Feb. 13–17, 2006.